Prediction of Distance to Maximum Intensity of Turbulence Generated by Grid Plate Obstacles in Explosion-induced Flows

A.M. Na'inna*[a], H.N. Phylaktou & G.E. Andrews[b]

[a] Air Force Institute of Technology, Nigerian Air Force, Nigeria
[b] Energy Research Institute University of Leeds, Leeds, United Kingdom

Abstract

The interaction of unburnt gas flow induced in an explosion with an obstacle results in the production of turbulence downstream of the obstacle and the acceleration of the flame when it reaches this turbulence. Currently, there are inadequate experimental measurements of these turbulent flows in gas explosions due to transient nature of explosion flows and the connected harsh conditions. Hence, majority of measurements of turbulent properties downstream of obstacles are done using steady-state flows rather than transient flows. Consequently, an empirical based correlation to predict distance to maximum intensity of turbulence downstream of an obstacle in an explosion-induced flow using the available steady state experiments was developed in this study. The correlation would serve as a prerequisite for determining an optimum spacing between obstacles thereby determining worst case gas explosions overpressure and flame speeds. Using a limited experimental work on systematic study of obstacle spacing, the correlation was validated against 13 different test conditions. A ratio of the optimum spacing from the experiment, x_{exp} to the predicted optimum spacing, x_{pred} for all the tests was between 2-4. This shows that a factor of three higher than the x_{pred} would be required to produce optimum obstacle spacing that will lead to maximum explosion severity. In planning the layout of new installations, it is appropriate to identify the relevant worst case obstacle separation in order to avoid it. In assessing the risk to existing installations and taking appropriate mitigation measures it is important to evaluate such risk on the basis of a clear understanding of the effects of

---

* Corresponding author. Tel:+2348030679898
E-mail address: Abdulmajid.nainna@airforce.mil.ng

separation distance and congestion. It is therefore suggested that the various new correlations obtained from this work be subjected to further rigorous validation from relevant experimental data prior to been applied as design tools.

Keywords: gas explosion; obstacles; obstacle spacing; turbulence intensity

1. Introduction

Gas explosion remains one of the major threats in oil, gas, chemical and other allied industries handling flammable materials and this often leads to loss of lives and properties. The severity of gas explosions is mostly expressed in terms of the overpressure generated because it determines the level of damage. Clancey (1975) shows that small overpressures could lead to a significant damage with an overpressure of 0.1 bar capable of causing serious structural damage. The generated overpressure in gas explosions is dependent upon number of factors which makes it a difficult task to estimate and one of such factors is obstacles (Yang *et al.* 2020). Many enclosures in onshore and offshore industrial sites in which gas explosions occur are likely to have obstructions in the form of process equipment, pipes, machinery, heat exchanger tubes and alike. The obstacles tend to wrinkle the propagating flame and make it more turbulent thereby increasing the reaction front area and the burning rate and hence the expansion rate and overpressure. Thus, obstacles are the most recognised means of increasing explosion severity (Hjertager 1984).

Many research investigations over the last 4 decades have identified a number of important obstacle variables that affect the severity of gas explosions in a congested region. These obstacle properties include the blockage ratio, size, shape, scale, location of obstacles, number of obstacles and spacing between the obstacles (Chapman and Wheeler, 1926; Harrison and Eyre, 1987; Hjertager *et al.,* 1988; Phylaktou, 1993; and Boeck *et al.* 2013). Although many

2

researchers have investigated the effect of multi-obstacles, the separation distance between obstacles has received little methodical investigation despite the general recognition of the significant role it plays in determining the explosion severity. Either too large or too small a separation distance between the obstacles would lead to lower explosion severity (Nainna *et al.* 2013). Therefore obstacles would need to have "optimal" separation distance to produce the worst case explosions overpressures and flame speeds. This is in compliance with the ATEX Directive (ATEX 1999) where worst case scenarios need to be used in assessing the severity of the hazard posed by gas explosions in process plant.

In the present perspective, obstacle should be considered as any object hindering and disturbing a flow field ahead of the flame front. The interaction of unburnt gas flow induced in an explosion with an obstacle results in the production of turbulence downstream of the obstacle and the acceleration of the flame when it reaches this turbulence. The turbulence level created is dependent upon the flow velocity and the geometry of confining boundaries.

Currently, there are inadequate experimental measurements of these turbulent flows in gas explosions due to transient nature of explosion flows and the connected harsh conditions. Therefore, the bulk of measurements of intensity of turbulence downstream of obstacles have involved steady-state flows in large wind tunnels such as Baines and Peterson (1951) among others. This has been recognised by Phylaktou and Andrews (1994) who presented a method to estimate the maximum intensity of turbulence behind a grid plate obstacle by an explosion-induced flow in terms of steady-state theory. Also, Cates and Samuels (1991) applied steady state flows to perform a simple assessment methodology for vented explosions. However, there is little or no study on the prediction of position to maximum intensity of turbulence in an obstacle-induced gas explosion.

The aim of this study therefore is to predict distance to maximum intensity of turbulence downstream of an obstacle in an explosion-induced flow using the available steady state experiments in the literatures. This would serve as a prerequisite for determining an optimum spacing between obstacles thereby determining worst case gas explosions overpressure and flame speeds.

2. Theoretical Background

In gas explosions with obstacles, the explosions overpressure and flame speeds are mainly determined by the intensity of turbulence, u'/U (defined as the ratio of the root-mean-square turbulence velocity u' to the mean velocity of the flow U) and its spatial distribution downstream of the obstacles. This is in addition to the geometry of the confinement. Presently, there exist limited data on the turbulence generated in transient flows with obstacles. Experiments from Hjertager *et al.* (1988) and Lindstedt and Sakhitharan (1998) are among the exceptionally few studies that focused on experimental turbulence measurements in gas explosions using multi-obstacle and single-obstacle configurations respectively. Thus, reliance on data from steady state non-reacting flow studies becomes necessary. So far, the bulk of turbulent measurements induced by obstacle (generally grid plates) have been made far downstream of obstacle mostly in a turbulent decay region, where the turbulence is isotropic i.e. 40-50 hole diameters downstream of the grid (Comte-Bellot *et al.* 1966). However, the decay region is away from the region of interest in the explosion hazards field since the maximum combustion rate normally occurs within a distance of 3 to 20 obstacle-hole diameters after the obstacle (Phylaktou and Andrews 1991).

Currently, there are few measurements of u'/U in the region immediately downstream of the grid (region of interest in gas explosions protection) using wind tunnel (steady flow) experiments by

Baines and Peterson (1951); Robinson and Kovitz (1975) and Checkel (1981) etc. Figure 1 shows an example of a near grid measurements of turbulence from the work of Baines and Peterson (1951). It is a plot of u'/U (measured on the centre-line of the grid holes) as a function of the axial distance, x normalised by the characteristic grid-scale b (b is defined as the width of the solid material between the grid holes). It is shown that the u'/U increases downstream of the obstacle prior to attaining a peak value some distance after it, and it then begins to decay at a more or less steady rate over a relatively long distance.
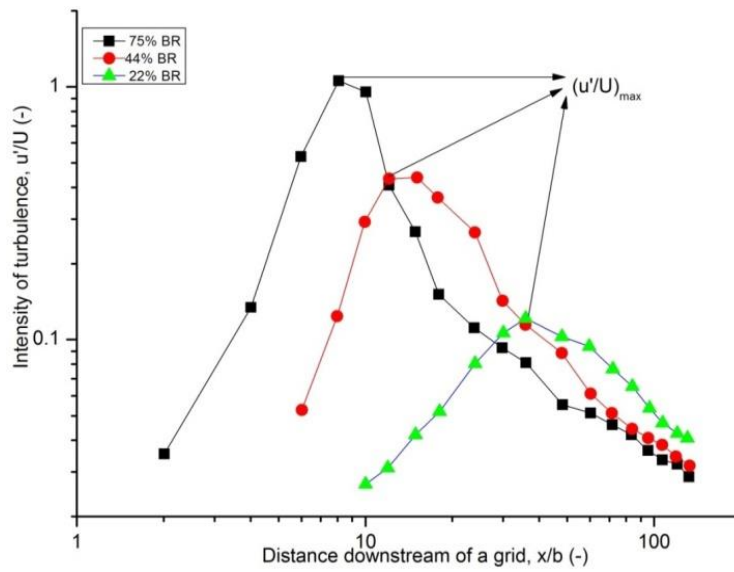
Figure 1: Turbulence intensity downstream of grid-plates of various obstacle blockages (Baines and Peterson 1951).

A method to predict the maximum u'/U generated downstream of a grid-plate obstacle by an explosion-induced flow is presented by Phylaktou and Andrews (1994) using a simple correlation given by Eq. 1 as,

u'/U = C_T $K^{0.5}$ (1)

where K is the obstacle pressure-loss coefficient and C_T is a turbulence generation constant.

Ward Smith (1980) expressed K in terms of obstacle blockage ratio, BR and coefficient of contraction (C_c) as,

$$K = \left(\frac{1}{C_c(1-BR)} - 1\right)^2 \tag{2}$$

In order to express K independent of C_c and only dependent upon the obstacle porosity ratio, p and geometrical characteristics of the obstacle, Ward Smith (1971) correlated an empirical data of C_c and combined with Eq. 2 to give a new value of K based on either thin/sharp edged obstacle (obstacle thickness to diameter ratio, t/d < 0.6) or thick/round edged obstacle (obstacle thickness to diameter ratio, t/d > 1) as Eq. 3 and 4 respectively.

$$K = \left[\frac{1}{0.608p(1-p^{2.6})\left[1+\left(\frac{t}{d}\right)^{3.5}\right]+p^{3.6}} - 1\right]^2 \quad \text{for t/d < 0.6 (thin/sharp obstacle)} \tag{3}$$

$$K = \left[\frac{1}{p\left[0.872-0.015\left(\frac{t}{d}\right)-0.08(d/t)\right](1-p^{3.3})+p^{4.3}[1+0.134(t/d)^{0.5}]^{-1}} - 1\right]^2 \quad \text{for t/d > 1 (thin/sharp obstacle)} \tag{4}$$

Equation 3 implies that the jet formed downstream of the orifice plate entry remains separated from the orifice wall and reattaches to the pipe wall only. This condition is known as a fully separated flow regime and in this case, there is no pressure loss. However, Eq. 4 indicates that the jet formed downstream of the orifice plate entry reattaches to both the orifice and pipe walls thereby leading to pressure loss. This condition is referred to as a fully reattached flow regime. Uncertainly arises for data within the range of 0.6 < t/d < 1, because the flow may reattach or not (marginally reattached flow) and hence omitted from the correlation (Ward Smith 1971).

The practical values of the constant C_T (from Eq. 1) were obtained using the measured data of the maximum u'/U downstream of grid plates in steady-state flows. The applicability of such

steady-state flow concepts was supported by experimental evidence. Phylaktou and Andrews (1994) determined two practical values of C_T as 0.225 and 0.076 for thin/sharp-edged obstacles and thick/round-edged obstacles respectively. The model was shown to predict available turbulence measurements in both transient (explosion-generated) and steady-state flows.

3.   Effects of Obstacle Separation Distance on Gas Explosions

From Fig. 1, it is evident that there is an "optimum" spacing for obstacles where each successive obstacle is placed just after position of peak turbulence so that it "sees" the maximum flame speed. This would in turn be expected to cause the maximum possible turbulence downstream of that obstacle and therefore overall would cause the fastest possible acceleration to the highest possible flame speed and hence highest overpressure. Conversely if the obstacle spacing is larger or smaller than the optimum, then flame acceleration would not be as severe as it should be and in overall the effect of repeat obstacles would be minimal. For closely separated obstacles, there would be no space for the development of the jet shear layers that generate turbulence downstream of the obstacle. But for widely separated obstacles, turbulence decay is encountered downstream of the first obstacle and this slows down the flame speed before approaching the second obstacle and this leads to reduced or no interaction (Lee and Moen 1980). The widely spacing between obstacles could serve as a safety gap between two congested process regions (Ma *et al.* 2014). The safety gap is an open space with no congestion deliberately placed in between congested process area and is one of the most effective and widely used safety measures. The safety gap basically interrupts a positive feedback mechanism in congested areas thereby eliminating the fluid-obstacle interaction thus preventing the generation of turbulence.

In compliance with the ATEX directive (1999), the worst case scenarios need to be used in assessing the severity of the hazard posed by gas explosions in process plant. Therefore an

optimum obstacle spacing corresponding to maximum explosion overpressure should be used in the general assessment of these phenomena.

Most gas explosion experiments were performed with multi-obstacle arrays of fixed obstacle spacing. Notable among these studies include that of: Chapman and Wheeler (1926); Kirkby and Wheeler (1931); Robinson and Wheeler (1933); Eckhoff *et al.* (1984); Lee *et al.* (1984); Hjertager *et al.* (1988); Moen *et al.* (1988); Peraldi *et al.* (1988); Chan and Greig (1989); Mackay *et al.* (1989); Phylaktou (1993); Sakthitharan (1995); Chan and Dewit (1996); Dorofeev *et al.* (1996); Gardner (1998); Alekseev *et al.* (2001); Kuznetsov *et al.* (2002); Lowesmith *et al.* (2011); Dong *et al.* (2012); Gamezo *et al.* (2013); Zipf Jr *et al.* (2014) and Boeck *et al.* (2017).

From the above experiments, the effects of obstacle separation distance on gas explosion severity could not be quantified because of the fixed obstacle spacing that was used within each set of experiments. As shown in Fig 2, the spacing between the obstacles in most of the experiments (over 90% of the data points) was within a range of just 1.2 to 8.8 characteristic obstacle scales with the exception of the works of Phylaktou (1993) and Gardner (1998). However, this is not within the range of 3 to 20 characteristic obstacle scales downstream of the grid where the maximum combustion rate usually occurs as given by Phylaktou and Andrews (1991).
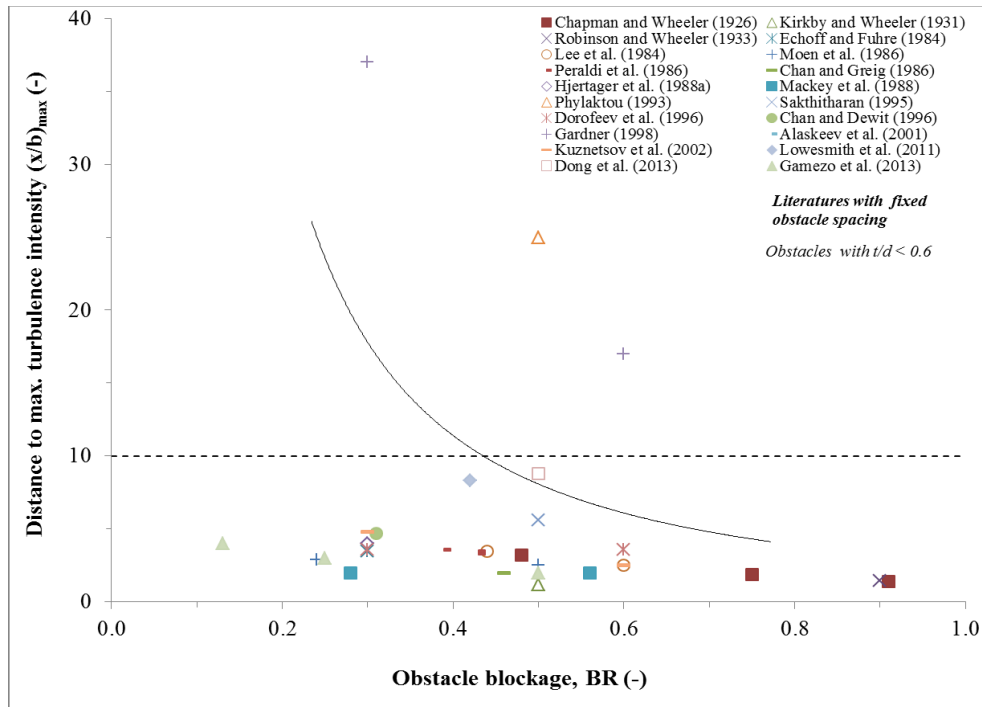
Figure 2. Relationship between dimensionless obstacle separation distance and obstacle blockage ratio for gas explosion studies with fixed obstacle spacing.

As part of wider assessment of the influence of congestions in gas explosions, a number of experimental explosion studies have demonstrated the effect of obstacle separation distance. These include the works of: Moen *et al.* (1980); Moen *et al.* (1982); Chan *et al.* (1983); Harrison and Eyre (1987); Lindstedt and Michels (1989); Teodorczyk *et al.* (1989); Mercx (1992); Beauvais *et al.* (1993); Obara *et al.* (1996); Mol'kov *et al.* (1997); Yu *et al.* (2002); Cicarelli *et al.* (2005); Teodorczyk *et al.* (2009); Rudy *et al.* (2011); Vollmer *et al.* (2011); Pang *et al.* (2012); Boeck *et al.* (2013); Porowski and Teodorczyk (2013); Wang *et al.* (2016); Li *et al.* (2016) and Ugarte *et al.* (2016). As shown in Fig 3, the bulk of the spacing (34 data points out of 45 data points) between obstacles of different blockage was within a range of 1.3 to 10 obstacle scales.

9
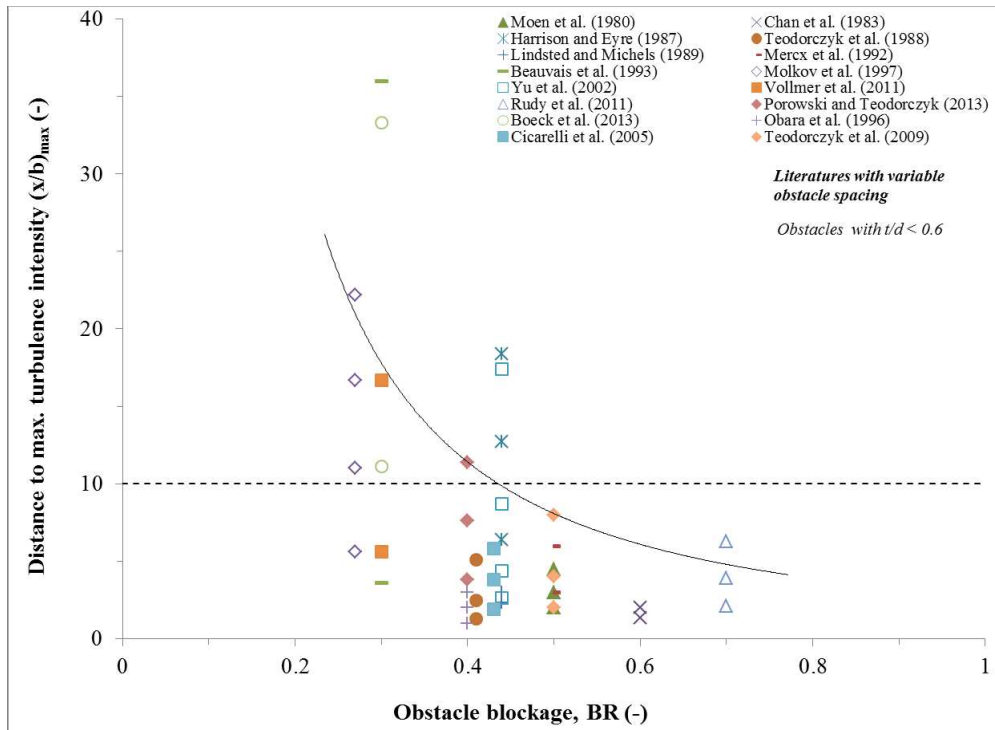
Figure 3. Relationship between dimensionless obstacle separation distance and obstacle blockage ratio for gas explosion studies with variable obstacle spacing.

Studies from Chan *et al.* (1983) ; Lindstedt and Michels (1989); Mercx (1992) and Vollmer *et al.* (2011) had their obstacles spaced over a short distance and also the obstacle spacing was varied over a limited range. Additionally, studies from Beauvais *et al.* (1993); Obara *et al.* (1996); Yu *et al.* (2002); Rudy *et al.* (2011); Vollmer *et al.* (2011) and Porowski and Teodorczyk (2013) involved obstacle-laden tubes where the separation distance of the multi-obstacles was partially explored. In most of the tests, deflagration to detonation transition, DDT had transpired. However, most of the industrial explosion incidents involved deflagrative rather than detonative propagation. Thus it is necessary to examine the effects of obstacle spacing in scenarios where the combustion remains in the deflagration regime without transition to detonation.

4.   Methodology in Obtaining Relevant Datasets

Phylaktou and Andrews (1994) obtained a correlation for u'/U immediately downstream of the grid (to produce maximum severity of explosion) against BR from the steady state flow experiments of Baines and Peterson (1951); Robinson and Kovitz (1975) and Checkel (1981). In the work of Na'inna (2013), additional works on measuring maximum u'/U behind a grid were sourced despite data insufficiency. These include the work performed by Tan-Atichat *et al.* (1982), Groth and Johansson (1988), DeOtte Jr *et al.* (1991) and Zhou and Lee (2004). Relevant datasets from the 5 researchers were extracted using GetData Software. Details of the experimental geometry, turbulence generating obstacles and other turbulence related properties are outlined in Table 1.

Table 1: *Overview of datasets from cold flow turbulence studies used in deriving the present correlations.*

Authors (-)	Obstacle (-)	BR (-)	d (m)	M (m)	b (m)	$(x/b)_{max}$ (-)	$(u'/U)_{max}$ (-)	t/d (-)
Baines and Peterson (1951)	Bi-plane bar lattice	0.61	0.0423	0.0677	0.0254	8.160	0.341	0.60
,,	Bi-plane bar lattice	0.44	0.0762	0.1016	0.0254	9.065	0.275	0.33
,,	Bi-plane bar lattice	0.44	0.2286	0.3048	0.0762	8.529	0.245	0.33
,,	Bi-plane bar lattice	0.44	0.0254	0.0339	0.0085	7.403	0.258	0.33
,,	Bi-plane bar lattice	0.23	0.1778	0.2032	0.0254	22.312	0.103	0.14
,,	Bi-plane bar lattice	0.89	0.0127	0.0381	0.0254	4.044	0.529	2.00
,,	Bi-plane bar lattice	0.75	0.0254	0.0508	0.0254	5.113	0.383	1.00
,,	Perforated plate	0.75	0.0254	0.0508	0.0267	8.072	1.057	0.19
,,	Perforated plate	0.44	0.0762	0.1016	0.0292	12.072	0.438	0.06
,,	Perforated plate	0.23	0.1778	0.2032	0.0343	35.885	0.121	0.03
Robinson and Kovitz (1975)	Perforated plate	0.74	0.0057	0.0112	0.0055	50.807	0.360	1.12
,,	Perforated plate	0.81	0.0057	0.0132	0.0075	47.381	0.460	1.12
,,	Perforated plate	0.89	0.0056	0.0170	0.0114	40.217	0.510	1.14
Checkel (1981)	Perforated plate	0.60	0.0100	0.0158	0.0063	3.487	0.580	0.50
,,	Perforated plate	0.60	0.0200	0.0316	0.0126	3.487	0.600	0.25
,,	Perforated plate	0.60	0.0025	0.0040	0.0016	13.498	0.100	2.00
,,	Perforated plate	0.60	0.0050	0.0079	0.0032	6.825	0.270	1.00
Tan-Atichat et al. (1981)	Perforated plate	0.37	0.0064	0.0070	0.0020	12.706	0.210	0.25
,,	Perforated plate	0.68	0.0016	0.0028	0.0013	11.725	0.290	1.01
Groth and Johansson (1988)	Square mesh grid	0.35	0.0042	0.0052	0.0010	18.200	0.140	0.24

| DeOtte et al. (1991) | Perforated plate | 0.75 | 0.0254 | 0.0502 | 0.0267 | 3.810 | 1.000 | 0.13 |
| Zhou and Lee (2004) | Perforated plate | 0.77 | 0.0250 | 0.0523 | 0.0286 | 5.254 | 0.132 | 0.20 |

5. Prediction of Distance to Maximum Intensity of Turbulence Downstream of Obstacle

Figures 4 and 5 show a plot of maximum u'/U against obstacle BR with the data separated into thin/sharp and thick/round geometries respectively. The acronyms BL, PP and SM stand for bi-plane lattice, perforated plate and square mesh respectively. For each geometry type, a strong dependence of the maximum u'/U on BR is indicated. The equations of the exponential correlations with R^2 values of 0.91 and 0.71 for t/d < 0.6 and t/d > 1 respectively indicating a very good fit are given as,

$$(u'/U)_{max} = 0.042e^{4.23BR} \qquad \text{for } t/d < 0.6 \quad \text{at} \quad BR \text{ of } 0.23 - 0.77 \tag{5}$$

$$(u'/U)_{max} = 0.018e^{3.90BR} \qquad \text{for } t/d > 1 \qquad \text{at} \quad BR \text{ of } 0.6 - 0.9 \tag{6}$$
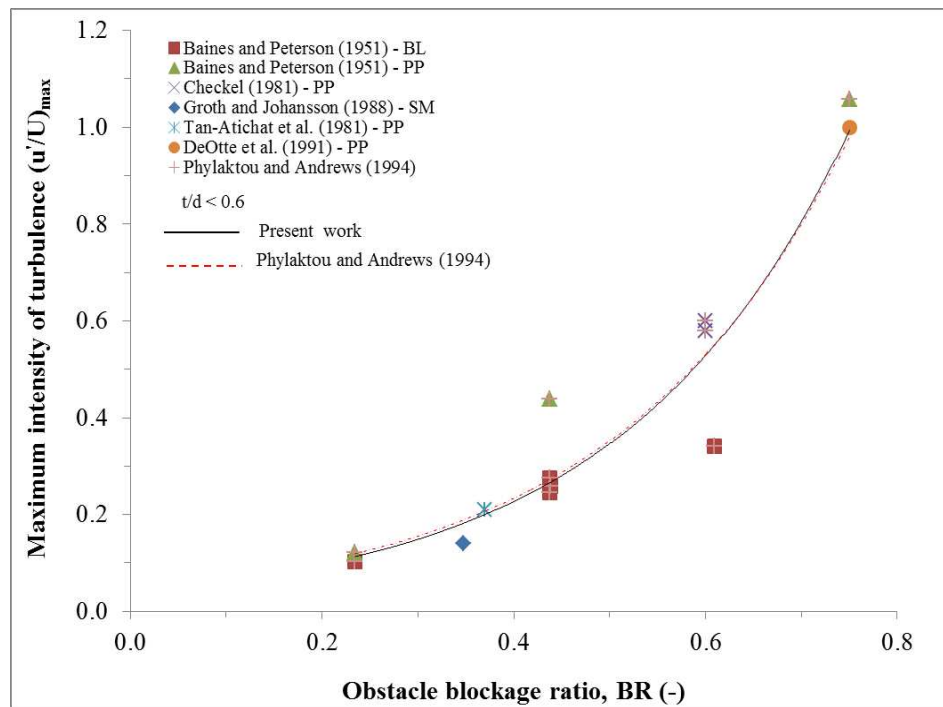
Figure 5. Maximum intensity of turbulence against obstacle blockage from cold flow turbulence

for t/d > 1.

Figure 6 shows the relationship between the dimensionless distances to peak intensity of turbulence, $(x/b)_{max}$ behind the grid against an obstacle blockage with t/d of less than 0.6 for the corresponding data used in Fig 4. The $(x/b)_{max}$ was found to increase with decrease in obstacle blockage. A power fit equation with an R^2 value of 0.76 to the data is given as,

$$(x/b)_{max} = 2.77BR^{-1.55} \qquad \text{for t/d < 0.6} \qquad \text{at} \quad BR \text{ of } 0.23 - 0.77 \qquad (7)$$

13
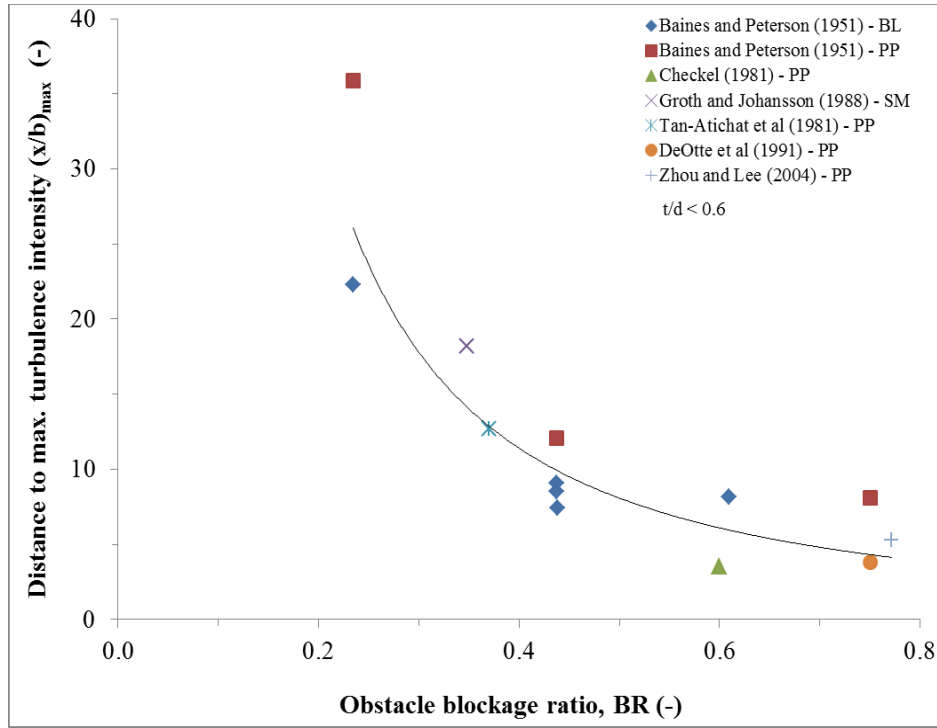
Figure 6. Position to (u'/U)$_{max}$ against obstacle blockage for grids of t/d <0.6.

The relation between the (x/b)$_{max}$ and obstacle blockage for grid plates with t/d > 1 is presented

in Fig. 7. With the exception of data of Robinson and Kovitz (1975); the scanty data were fitted

with a power fit equation (with R^2 value of 0.59) applicable to an orifice blockage of 0.6 to 0.9

as,

$$(x/b)_{max} = 3.10BR^{-2.40} \qquad \text{for t/d > 1} \qquad \text{at BR of 0.6 - 0.9} \qquad (8)$$

The omission of the data points from the work of Robinson and Kovitz (1975) in correlating Eq.

8 is due to high values of (x/b)$_{max}$ for high obstacle blockage ratio which is not supposed to be

the case. The (x/b)$_{max}$ is expected to decrease with increase in obstacle blockage due to reduction

in obstacle-hole diameter as indicated in Fig 6. A likely reason for this discernible discrepancy

could be attributed to the use of a cylindrical geometry used by Robinson and Kovitz (1975)

whereas the remaining authors used wind tunnels to perform their experiments. As the turbulence

14

levels were increased by increasing the obstacle blockage ratio, the explosion tubular geometry prevented the turbulence from spreading radially and forced it to spread axially over a long distance downstream of the grid.
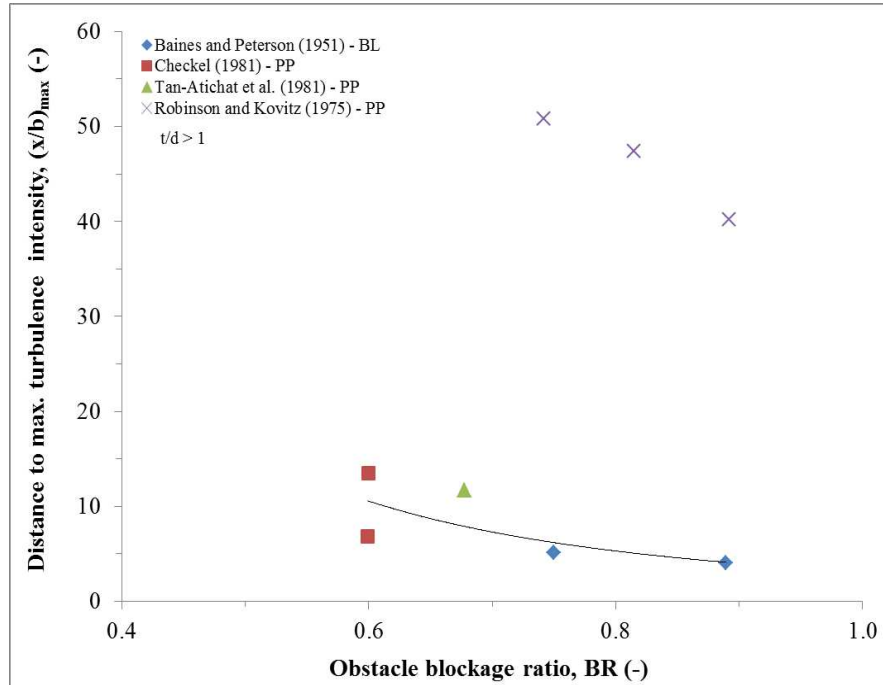
Figure 7. Position to $(u'/U)_{max}$ against obstacle blockage for grids of t/d > 1.

Generally, the correlations derived based on t/d < 0.6 (Eqs 5 and 7) and t/d > 1 (Eqs 6 and 8) are limited to BR of 0.23 – 0.77 and 0.6 – 0.9 respectively.

6.   Relationship between $(u'/U)_{max}$ and $(x/b)_{max}$

The region of major concern in explosion hazards is the region of maximum turbulence that is shown in Fig. 1 to occur at some distance behind the grid. In an explosion situation, the highest burning rate (and hence peak rate of generation of overpressure) will transpire at the position of maximum turbulence intensity, and it is therefore this region that should guide the protection and mitigation requirements in a system.

15

The position to maximum u'/U is of great concern in multi-obstacle explosions. This would determine the spacing between the obstacles in order to determine the utmost severity of explosions. From the existing data of turbulence measurement immediately behind a grid, a correlation between dimensionless distance to maximum intensity and the maximum intensity of turbulence was formed for thin/sharp and thick/round obstacles as shown in Figs 8 and 9 respectively. The $(u'/U)_{max}$ with dependence on obstacle BR would be obtained from either Eq. 5 or 6. The equations best fitted for the correlations are given as,

$$(x/b)_{max} = 3.87 \left(\frac{u'}{U}\right)_{max}^{-0.77} \quad \text{for } \frac{t}{d} < 0.6 \quad \text{at } (u/U)_{max} \text{ of } 0.12 - 1.06 \tag{9}$$

$$(x/b)_{max} = 2.99 \left(\frac{u'}{U}\right)_{max}^{-0.70} \quad \text{for } \frac{t}{d} > 1 \quad \text{at } (u/U)_{max} \text{ of } 0.1 - 0.53 \tag{10}$$

The implication of Eq. 9 and 10 is that in real multi-obstacle explosions, both the u'/U_{max} and its corresponding x/b could be predicted and compared with the actual values given in the experiments to ascertain whether maximum severity of explosions is achieved or not.
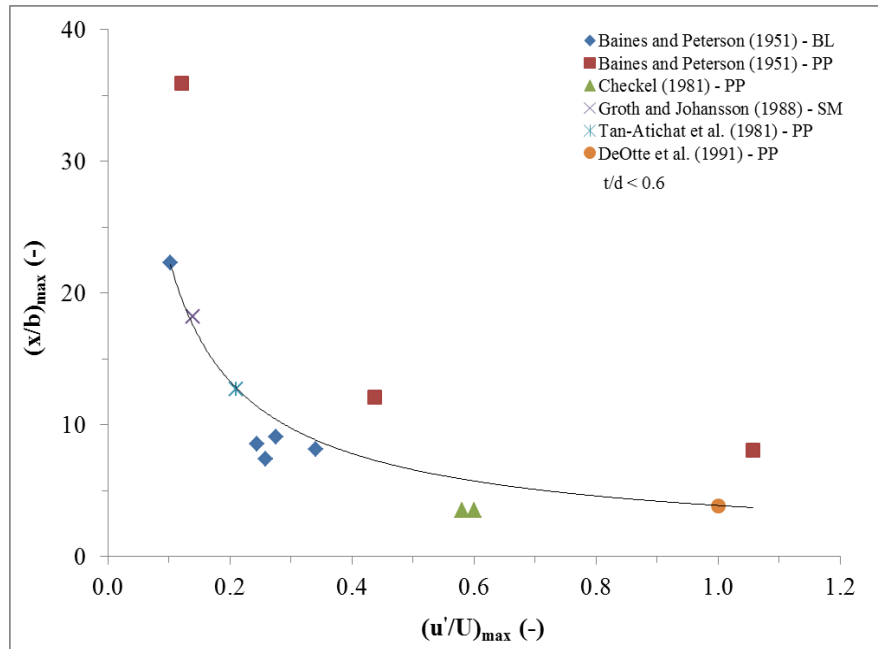
Figure 8. Correlation between maximum intensity of turbulence and its distance for grid plates with t/d < 0.6.

16
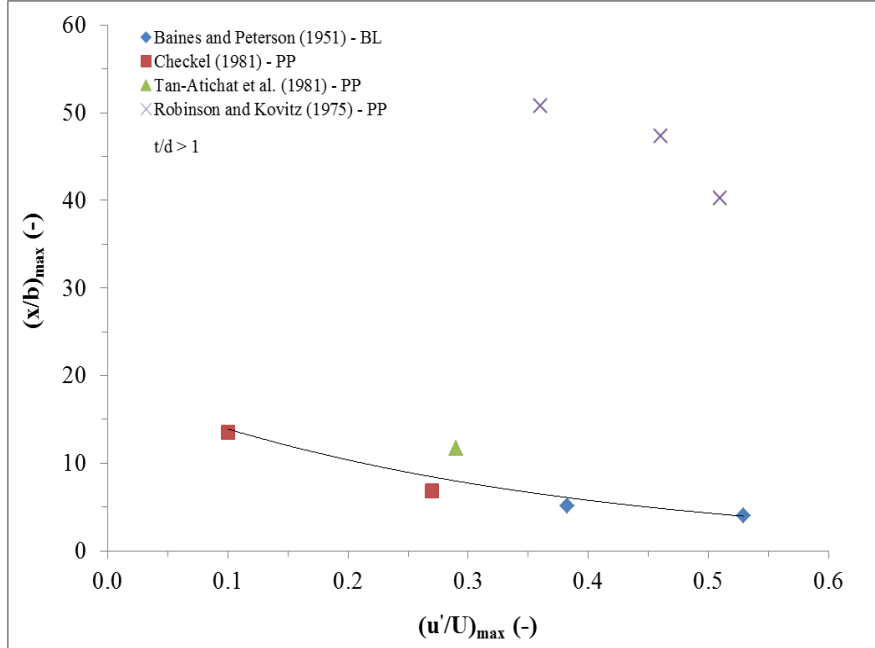
Figure 9. Correlation between maximum intensity of turbulence and its distance for grid plates with t/d > 1.

7.   Position of Maximum Intensity of Turbulence of Grid Plates and Free Jet Theory

From free jet theory, the maximum intensity of turbulence on the centreline of an orifice plate is anticipated to occur after the completion of the jet potential core where the interior edges of the surrounding shear region meet (Beer and Chigier 1983). The length of the potential core is expressed in terms of jet diameter, d_{jet}. The d_{jet} of a flow through an orifice is the diameter of the vena contracta (given in Eq. 11) which is dependent on the open flow diameter of an obstacle, d and the coefficient of contraction, C_c as

$$C_c = \frac{A_{vc}}{A_1} \qquad (11)$$

Prior to obtaining d_{jet}, the values of K for the geometries in Fig. 4 were calculated using Eq. 3 followed by determining the appropriate value of C_c for each geometry using Eq. 2. Figure 10

shows a plot of the position of maximum intensity of turbulence as a function of the jet diameter, x_{max}/d_{jet} against the obstacle blockage ratio, BR.
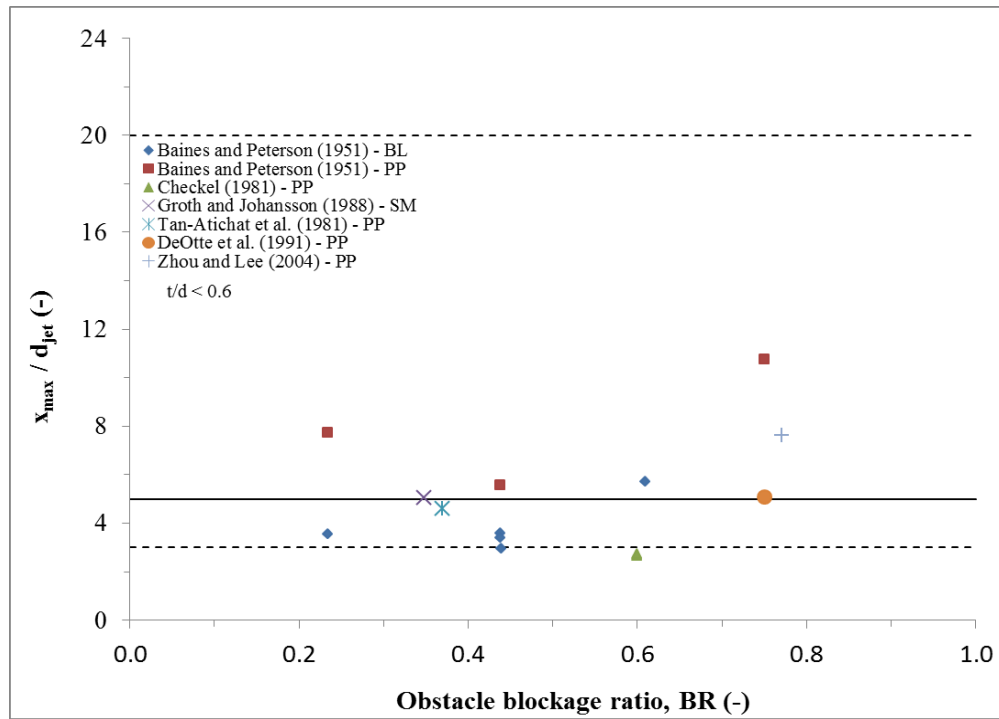
Figure 10. Distance to $(u'/U)_{max}$ expressed in terms of jet diameter versus obstacle blockage.

It was observed that the, x_{max}/d_{jet} is independent of the obstacle blockage and hence the intensity of turbulence. The whole data used in the plot fell within a region of 3 to 10 jet diameters with the majority been between 3 to 6 jet diameters. The average position of u'/U_{max} for all the data points shown as a solid line is five and this agrees well with the expectancy of peak turbulence intensity been at or subsequent to the completion of the potential core generally taken to be 4-5 jet diameters long (The dotted lines at 3 and 20 d_{jet} indicate the range at which the maximum flame speed occurred downstream of the obstacle in a series of explosion test in tubes with grid plates (Phylaktou and Andrews 1991).

To further substantiate the relationship between the position of maximum intensity of turbulence and the free jet theory, the length of the potential core (4.5 d_{jet}) could be equated to the distance to $(u'/U)_{max}$.
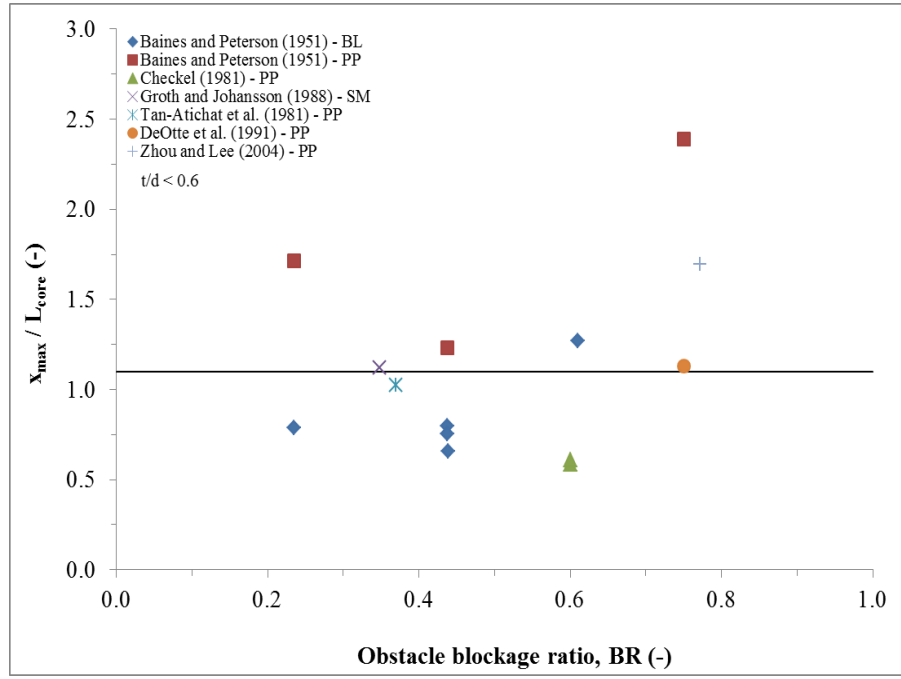
Figure 11. x_{max} to L_{core} relationship against obstacle blockage.

Figure 11 shows the ratio of x_{max}/L_{core} against the obstacle blockage for all the geometries in Fig. 4. The ratio x_{max}/L_{core} was found to be independent of the blockage just like x_{max}/d_{jet}. The entire data points are situated within a range of x_{max}/L_{core} of 0.6 to 2.4 with the majority been between 0.6 to 1.2. The solid line shown in the plot is the average of the x_{max}/L_{core} for all the data points and it was obtained to be around unity. This suggests that the position to $(u'/U)_{max}$ could be ascertained using free jet theory by obtaining the length of the potential core.

8.   Limited Validation with the Available Experimental Data

The separation distance (pitch) between obstacles is an area that has received little attention by explosion researchers despite the general recognition of the important role it plays in determining the explosion severity. With reference to Fig. 1, it is discernible that either too large or too small

separation distance between the obstacles would lead to lower intensity of turbulence and hence explosion severity whereas optimum obstacle spacing would produce the highest explosion severity. Based on, ATEX directives, only the optimum obstacle spacing producing the worst case scenarios will be applicable in gas explosion risk assessment and preventive/mitigative measures.

To the authors' knowledge, the only available experimental work that systematically studied the influence of spacing between obstacles in gas explosions in order to determine the worst case separation that will produce the maximum explosion severity is that of Na'inna (2013). Na'inna (2013) used a long vented cylindrical vessel 162 mm internal diameter with an overall length to diameter ratio (L/D) of 27.7 to perform the experimental study. The vessel was closed at the ignition end and its open end connected to a large cylindrical dump-vessel with a volume of 50 m^3. The spacing between the two obstacles in the test vessel was systematically varied from 0.25 m to 2.75 m. The influence of obstacle spacing was studied with obstacles of different blockage ratios, shapes, number and scale. Tests were carried out with methane, propane, ethylene and hydrogen mixtures with air. Table 2 gives an overview of the obstacles used in the study. The pressure loss coefficient across the obstacle, K_{ob} was calculated from Eq. 3 since the obstacle thickness to diameter, t/d is less than 0.6 (thin/sharp obstacles). The integral length scale, ℓ which determines the level of turbulence, is taken to be half the obstacle length scale, b.

Table 2: *Basic design parameters for the obstacles used by Na'inna (2013).*

Shape	BR	N_b/N_h	t/d	K_{ob}	b	ℓ
(-)	(-)	(-)	(-)	(-)	(mm)	(mm)
Hole-type	0.2	1	0.02	0.26	24.4	12.2
"	0.3	1	0.02	0.76	33.2	16.6
"	0.4	1	0.03	1.80	42.8	21.4
"	0.4	4	0.05	1.80	22.0	11.0
"	0.4	16	0.10	1.80	5.4	2.7
Flat-bar	0.2	1	0.05	0.26	25.6	12.8
"	0.2	2	0.11	0.26	12.8	6.4
"	0.2	4	0.17	0.26	6.4	3.2
"	0.3	1	0.05	0.76	38.5	19.3

In total, over 40 tests were carried out demonstrating 13 different test conditions. Table 3 shows a list of the tests carried out as part of this work. Also shown in Table 3 is the prediction of distance to maximum intensity of turbulence, $(x_s/b)_{pred}$ obtained from Eq 7 as well as the experimental optimum obstacle spacing $(x_s/b)_{exp}$ leading to maximum explosion overpressure and flame speed. A ratio of x_{exp} to x_{pred} for all the tests in the research was between 2- 4 which is an average of 3. This shows that a factor of 3 higher than the x_{pred} from Eq. 7 would be required to produce optimum obstacle spacing that will lead to worst case explosion overpressure and flame speed. Although the present tests followed a similar profile to that of turbulence growth and decay, with the maximum however occurring at a further distance from the obstacle than suggested by the Baines and Peterson (1951) data for cold flows. A possible explanation for the non-correspondence between the cold flow position of maximum turbulence and the worst case obstacle separation distance is that once the flame moves through the obstacle the whole of the generated turbulence profile is detached from the obstruction it is in fact conveyed forward (whilst at the same time being consumed) by the advancing flame front.

Table 3: Comparison between the predicted and experimental distances to maximum turbulence intensity

Test (-)	Fuel (-)	Conc. (%)	BR (-)	Shape (-)	b (m)	$(x_s/b)_{pred}$ (-)	x_{pred} (m)	$(x_s/b)_{exp}$ (-)	x_{exp} (m)	x_{exp}/x_{pred} (-)
1	CH_4	10	0.3	1-hole	0.0332	17.9	0.59	52.7	1.75	3
2	CH_4	7	0.3	1-hole	0.0332	17.9	0.59	37.6	1.25	2
3	C_3H_8	3	0.3	1-hole	0.0332	17.9	0.59	67.7	2.25	4
4	C_2H_4	4.3	0.3	1-hole	0.0332	17.9	0.59	67.7	2.25	4
5	H_2	15	0.3	1-hole	0.0332	17.9	0.59	67.7	2.25	4
6	CH_4	10	0.4	1-hole	0.0428	11.5	0.49	34.9	1.50	3
7	CH_4	10	0.2	1-hole	0.0244	33.6	0.82	92.4	2.25	3
8	CH_4	10	0.3	1-bar	0.0385	17.9	0.69	45.5	1.75	3
9	CH_4	10	0.2	1-bar	0.0256	33.6	0.86	87.9	2.25	3
10	CH_4	10	0.2	2-bar	0.0128	33.6	0.43	97.7	1.25	3
11	CH_4	10	0.2	4-bar	0.0064	33.6	0.22	78.1	0.50	2
12	C_3H_8	4.5	0.2	2-bar	0.0128	33.6	0.43	136.7	1.75	4
13	C_3H_8	4.5	0.2	4-bar	0.0064	33.6	0.22	78.1	0.50	2

Table 4 gives an overview of turbulence combustion parameters which are aimed at giving a detailed physics of turbulent gas explosions rather than the conventional flame speeds and

explosion overpressures. A comprehensive review on the techniques used to calculate each parameter in the present research was given by Na'inna *et al.* (2016).

Table 4: *Comparison between maximum predicted and experimental overpressures*

Test	S_L	$(u'/U)_{max}$	$U = S_g$	u'	R_ℓ	S_T/S_L	S_{fexp}	M	P_{pred}	P_{exp}
(-)	(m/s)	(-)	(m/s)	(m/s)	(-)	(-)	(m/s)	(-)	(bar)	(bar)
1	0.45	0.149	153	23	34813	110	486	1.43	2.35	2.68
2	0.24	0.149	93	14	17607	95	280	0.82	1.04	0.73
3	0.25	0.149	87	13	16990	89	275	0.81	1.01	0.85
4	0.30	0.149	89	13	15655	81	276	0.81	1.02	0.98
5	0.41	0149	77	12	11504	59	630	1.85	3.37	3.64
6	0.45	0.228	160	36	68502	168	716	2.11	4.00	3.38
7	0.45	0.098	79	8	7546	42	362	1.06	1.54	1.16
8	0.45	0.149	117	17	35421	97	463	1.36	2.20	2.42
9	0.45	0.098	118	12	12528	58	412	1.21	1.86	1.29
10	0.45	0.098	91	9	4535	38	386	1.14	1.69	1.18
11	0.45	0.098	56	5	1512	22	357	1.05	1.51	1.11
12	0.53	0.098	144	14	9261	54	910	2.68	5.46	6.04
13	0.53	0.098	88	9	2600	29	578	1.70	3.00	4.48

By considering the obstacle as an orifice plate and using the procedures described in the British Standard (2003), the maximum unburnt gas flow velocity ahead of the flame, S_g was calculated from the experimental measured static pressure difference across the obstacle using static pressure tappings at 1D and 0.5D upstream and downstream of the obstacle respectively. By considering the area of the tube, A, mass flow rate, $\dot{m}$ and density, ρ the S_g is thus given as,

$$S_g = \frac{\dot{m}}{\rho A} \tag{12}$$

The $(u'/U)_{max}$ leading to maximum severity in explosions was obtained as the product of the turbulence generation constant, C_T and the square root K (Phylaktou and Andrews 1994). For thin/sharp (t/d < 0.6) obstacle, C_T is 0.225 whereas K is as given in Eq 3.

In general, fluid flow either laminar or turbulent is characterised by a non-dimensional number called Reynolds number, R_ℓ. Most of the real combustion systems operate in turbulent regimes with values of R_ℓ ranging from 250 to 25,000 (Andrews *et al.* 1975). In vapour cloud explosions

with pipe arrays, Catlin and Johnson (1992) estimated R_ℓ in the order of 70,000. For a given u′, integal length scale, ℓ (ℓ = 0.5b) and kinematic viscosity, v; the R_ℓ in the present work is calculated as,

$$R_\ell = (u'\ell/v)$$ (13)

The interaction of a flame with an obstacle results in an increase of the flame area. The flame shape distorts as it follows the turbulent flow patterns downstream of the obstacle. There are several models in the literature to measure the turbulent burning velocity, S_T. The S_T that results is therefore greater than the laminar value, S_L. In the present study, the S_T is calculated using Eq 14 as given by Phyaktou and Andrews (1995).

$$\frac{S_T}{S_L} = 1 + 0.67\left(\frac{u'}{S_L}\right)^{0.47} R_l^{0.31}$$

(14)

One of the most typical reasons to induced turbulence combustion is the pressure wave-flame interaction. Flame propagation in pipes relies intensely on acoustical wave disturbance through pipe particularly on rarefaction wave action reflected from the vent end. In case of tests in a tube with one end opened as in the case of Na'inna (2013), the influence of the rarefaction wave that moves toward the closed end and its influence on overpressure was apparent. This was more discernible in terms of fuel types and mixture reactivities. Generally, rarefaction wave has a great effect on flame configuration and flame propagation behaviour. When encountered with rarefaction wave, the flame is induced to quickly change from laminar to turbulence due to rarefaction wave-flame interaction. During the course of flame propagation, the turbulence intensity is strengthened. Sun *et al.* (2005) and Chen *et al.* (2007) experimentally studied the influence of rarefaction wave on flame structure and propagation using stoichiometric premixed

23

methane-air and propane-air respectively. In both studies, rarefaction wave was produced due to the rupture of membrane separating the main combustion and the additional rooms, which made laminar combustion transform into turbulent after the rarefaction wave surpassed the combustion wave. The membrane in the present study could be regarded as the obstacle positioned 1 m downstream of the spark plug where the flame propagation from spark initiation is laminar and transits to turbulent immediately downstream of the obstacle.

In vapour cloud explosions, it's common to assume that the overpressure is proportional to the square of the flame speed (Taylor and Hirst 1989; Harris and Wickens 1989). The assumption was based on simplified acoustic theory given by Taylor (1946) in terms of flame speed and Mach number, M (ratio of the average experimental flame speed, S_{fexp} to an ambient speed of sound of 340 m/s). At ambient atmospheric pressure and specific heat constant, γ of 1.4, then the predicted overpressure, P_{pred} is given in Eq. 15.

$$P_{red} = \frac{2\gamma M^2}{1+M} \tag{15}$$

Figure 12 shows a plot of predicted overpressure, P_{pred} obtained from Eq. 15 against the experimental overpressure, P_{exp} from the work of Na'inna (2013). There is a good agreement between the P_{pred} and P_{exp} with an R^2 value of 0.9. A similar approach was used by Harrison and Eyre (1987) to compare measured flame speeds and overpressures during low-energy ignition tests using a large scale wedge-shaped enclosure with a simplified acoustic flame theory and a good agreement was obtained.

Effects of obstacle separation distance on gas explosions with obstacles of variable blockage, size, scale and fuel types by Na'inna (2013)

$R^2 = 0.8966$

Predicted explosion overpressure using acoustic flame theory

$$P_{red} = \frac{2\gamma M^2}{1 + M}$$
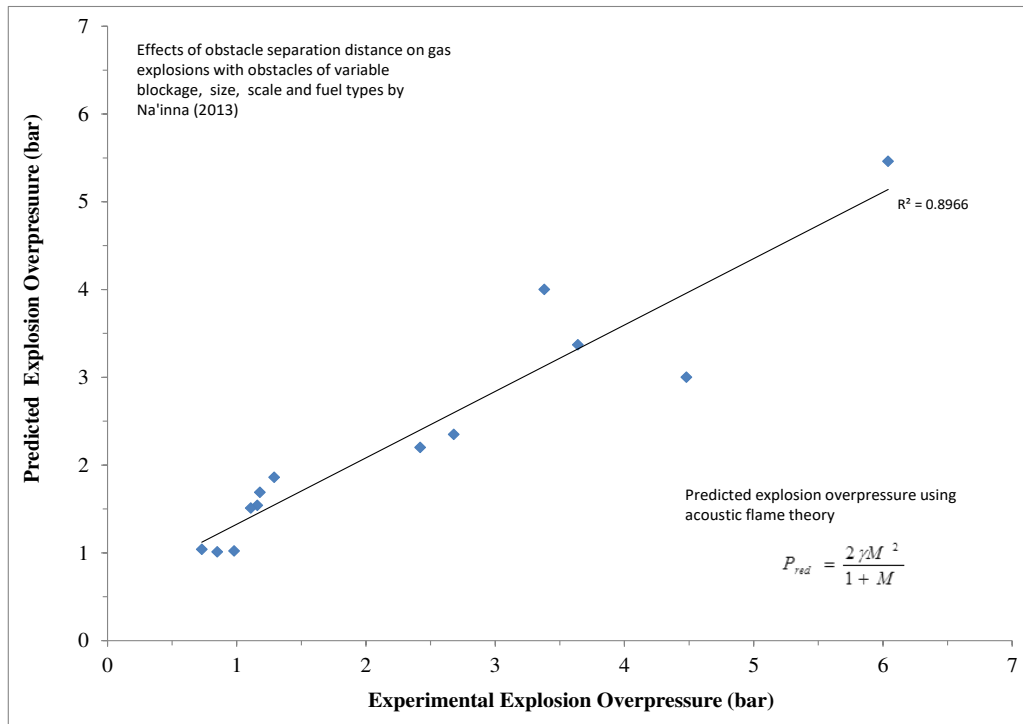
Figure 12: Comparison between predicted and experimental explosion overpressures.

The implication of this good agreement was that the mechanism of pressure generation in Na'inna (2013) is the same as that of vapour-cloud explosions, i.e. the pressure rise was due mainly to the inertia of the gas immediately ahead of the flame, and that it was not significantly influenced by the confinement offered by the tubular geometry. It would however be expected that in a largely-confined system such as the author's arrangement (a tube with an open far-end), the P_{max} would be a function of the net volume increase in the system. This is the balance between volume generation by the combustion process and volume reduction by venting, and therefore the pressure would not simply be a function of the flame speed as in a vapour cloud explosion. However, the pressure records at the end of tube and that of dump-vessel indicated little pressure difference between the two vessels and therefore limited venting was taking place at the time of maximum flame acceleration. Therefore the overpressures measured in the experiments were due to the high flame speeds which were caused by the obstacle induced turbulence which itself on the flame speeds associated flow velocities upstream of the obstacle.

9.   Conclusion

The interaction of unburnt gas flow induced in an explosion with an obstacle results in the production of turbulence downstream of the obstacle and the acceleration of the flame when it reaches this turbulence. Currently, there is very limited data on the turbulence generated in transient flows so reliance on data from steady state non-reacting flow studies becomes imperative. From turbulence intensity profile, it is discernible that there is an "optimum" spacing for obstacles where each successive obstacle is placed just after position of peak turbulence so that it "sees" the maximum flame speed. This would in turn be expected to cause the maximum possible turbulence downstream of that obstacle and therefore overall would cause the fastest possible acceleration to the highest possible flame speed and hence highest overpressure. Despite the role of obstacle spacing in determining the explosion severity, yet it has received little attention by gas explosion researchers.

A correlation was developed and applied to predict the position to maximum intensity of turbulence downstream of an obstacle, x_{max} dimensionalised with obstacle scale, b as a function of obstacle blockage ratio, BR, using steady state experiments from the limited available data in the literature as,

$$(x/b)_{max} = 2.77BR^{-1.55} \quad \text{for} \ t/d < 0.6 \ \text{(thin/sharp obstacles)}$$

$$(x/b)_{max} = 3.10BR^{-2.40} \quad \text{for} \ t/d > 1 \ \text{(thick/round obstacles)}$$

The correlation for thin/sharp obstacles was found to be in agreement with free jet theory for the position of maximum turbulence intensity given as 4.5 jet diameters (d_{jet}). Also, the correlation for thin/sharp obstacles was validated against a limited experimental work that systematically

studies the effects of obstacle separation distance on gas explosions. With 13 different test conditions ranging from fuel type, fuel concentration, obstacle blockage, obstacle shape and obstacle scale, the ratio of the optimum spacing from the experiment, x_{exp} to the predicted optimum spacing, x_{pred} for all the tests was between 2-4 which is an average of three. This shows that a factor of three higher than the x_{pred} would be required to produce optimum obstacle spacing that will lead to worst case explosion overpressure and flame speed. Although the present tests followed a similar profile to that of turbulence growth and decay, with the maximum however occurring at a further distance from the obstacle than suggested by studies from cold flow turbulence. It is suggested that this may be due to the convection of the turbulence profile by the propagating flame.

In compliance with the ATEX Directive, the worst case scenarios need to be used in assessing the severity of the hazard posed by gas explosions in process plant. Therefore an optimum obstacle spacing corresponding to maximum explosion overpressure should be used in the general assessment of these phenomena. It is suggested that the various new correlations obtained from this work be subjected to further rigorous validation from relevant experimental data prior to been applied as design tools.

Acknowledgements

References

Alekseev, V. I., Kuznetsov, M. S., Yankin, Y. G. and Dorofeev, S. B. 2001. Experimental study of flame acceleration and the deflagration-to-detonation transition under conditions of transverse venting. *J. Loss Prevent. Proc. Ind.,* 14, 591.

Andrews, G. E., Bradley, D. and Lwakabamba, S. B. 1975. Turbulence and turbulent flame propagation - A critical appraisal. *Combust. Flame,* 24, 285.

ATEX 1999. (Explosive Atmosphere) *1999/92/EC*, European Commission.

Baines, W. D. and Peterson E.G. 1951. An investigation of flow through screens. *Trans. ASME,* 73, 167.

Beauvais, R., Mayinger F. and Strube G. 1993. Severe Accident in a light water reactor: Influence of elevated initial temperature on hydrogen combustion. *ASME/JSME Nucl. Eng. Conf.,* 1,425.

Beer, J. M. and Chigier. N. A. 1983. *Combustion aerodynamics* (Ed). Applied science publishers, Essex.

Boeck, L. R., Hasslberger J., Ettner F. and Sattelmayer T. 2013. Investigation of peak pressures during explosive combustion of inhomogeneous hydrogen-air mixtures. *In: Proc. of the Seventh Int. Sem Fire & Explosion Hazards (ISFEH7),* Research Publishing, Providence, pp. 959–965.

Boeck, L.R., Kellenbergerb M., Rainsfordb G. and Ciccarell, G. 2017. Simultaneous OH-PLIF and Schlieren Imaging of Flame Acceleration in an Obstacle-Laden Channel. *Proc. Combust. Inst.*, 36, 2807.

British Standard BS5167-2. 2003. *Measurement of fluid flow by means of pressure differential devices inserted in circular cross-section conduits running full - Part 2: Orifice plates (ISO 5167-2:2003).* European Committee for Standardization. Brussels.

Cates, A. and B. Samuels. 1991. A simple assessment methodology for vented explosions. *J. Loss Prevent. Process Ind.,* 4, 287.

Catlin, C.A. and Johnson, D.M. 1992. Experimental scaling of the flame acceleration phase of an explosion by changing fuel gas reactivity. *Combust. Flame,* 88, 15.

Chan C.K. and Dewit, W.A. 1996. Deflagration-to-detonation transition in end gases. *Proc. Combust. Inst.*, 26, 2679.

Chan, C., Moen, I. O. and Lee, J. H. S. 1983. Influence of confinement on flame acceleration due to repeated obstacles. *Combust Flame,* 49, 27.

Chan, C. K. and Greig D.R. 1989. The structures of fast deflagrations and quasi-detonations. *Proc. Combust. Inst.,* 22,1733.

Chapman, W. R. and Wheeler R.V. 1926. The propagation of flame in mixtures of methane and air. Part IV. The effect of restrictions in the path of the flame. *J. Chem. Soc.,* 37, 2139.

Checkel, M. D. 1981. *Turbulence enhanced combustion of lean mixtures*. PhD thesis, University of Cambridge.

Chen, X., Sun, J., Lu, S., Chu, G., Yao, L. and Liu, Y. 2007. Influence of rarefaction wave on premixed flame structure and propagation behaviour. *Prog. Natural Sci.* 17, 328.

Ciccarelli, G., Fowler C. J. and M. Bardon. 2005. Effect of obstacle size and spacing on the initial stage of flame acceleration in a rough tube. *Shock Waves,* 14,161.

Clancey, V. J. 1975. The phenomenology of vapour cloud explosions in free space. *In: Europ. Symp. Comb., French Section, Comb. Inst.,* Paris. p.p.238.

Comte-Bellot, G., Eacute, V and Corrsin S. 1966. The use of a contraction to improve the isotropy of grid-generated turbulence. *J. Fluid Mech.,* 25, 657.

Deotte Jr, R.E., Morrison G.L., Panak D.L. and Nail G.H. 1991. 3-D laser doppler anemometry measurements of the axisymmetric flow field near an orifice plate. *Flow Meas. Instrum.,* 2,115.

Dong, C., Bi, M. and Zhou, Y. 2012. Effects of obstacles and deposited coal dust on characteristics of premixed methane–air explosions in a long closed pipe. *Saf. Sci.,* 50, 1786.

Dorofeev, S.B., Sidorov V.P., Dvoinishnikov A.E. and Breitung W. 1996. Deflagration to detonation transition in large confined volume of lean hydrogen-air mixtures. *Combust. Flame,* 104,95.

Eckhoff, R.K., Fuhre K., Guirao, C.M. and Lee, J.H.S. 1984. Venting of turbulent gas explosions in a 50 m^3 chamber. *Fire Saf. J.,* **7**, 191.

Gamezo, V.N., Zipf, R.K., Mohamed, K.M., Oran, E.S. and Kessler, D.A. 2013. DDT Experiments with Natural Gas-Air Mixtures. *In: Proc. of the Seventh International Seminar on Fire & Explosion Hazards (ISFEH7).* Research Publishing, Providence, pp.729-738.

Gardner, C. L. 1998. *Turbulent combustion in obstacle-accelerated gas explosions – The influence of scale*. PhD thesis, University of Leeds.

Groth, J. and Johansson, A.V. 1988. Turbulence reduction by screens. *J. Fluid Mech.,* 197,139.

Harris, R. J. and Wickens, M. J. 1989. Understanding vapour cloud explosions-an experimental study. *In: 55th Autumn Meeting: The Institution of Gas Engineers.* The Institution of Gas Engineers, Kensington.

Harrison, A. J. and Eyre, J.A. 1987. The effect of obstacle arrays on the combustion of large premixed gas/air clouds. *Combust. Sci. Technol.,* 52,121.

Hjertager, B. H. 1984. Influence of turbulence on gas explosions. *Journal of Hazardous Materials,* **9**(3), pp.315-346.

Hjertager, B. H., K. Fuhre And M. Bjørkhaug. 1988. Concentration Effects on Flame Acceleration by Obstacles in Large-Scale Methane-Air and Propane-Air Vented Explosions. *Combust. Sci. Technol.,* 62, 239.

Kirkby, W.A. and Wheeler, R.V. 1931. Explosions in closed cylinders. Part V. The effect of restrictions. *J. Chem. Soc.,* Part V, 2303.

Kuznetsov, M., Alekseev, V., Yankin, Y. and Dorofeev, S. 2002. Slow and fast deflagrations in hydrocarbon-air mixtures. *Combust. Sci.Tech.,* 174,157.

Lee, J.H.S., Knystautas, R. and Freiman, A. 1984. High speed turbulent deflagrations and transition to detonation in H_2O- air mixtures. *Combust. Flame,* 56, 227.

Lee, J. H. S. and Moen, I.O. 1980. The mechans of transition from deflagration to detonation in vapor cloud explosions. *Prog. Energy Combust. Sci.,* 6, 359.

Li, J., Ma. G., Hao, H. and Huang, Y. 2016. Gas explosion analysis of safety gap effect on the innovating FLNG vessel with a cylindrical platform. *J. Loss Prevent. Process Ind.,* 44, 1.

Lindstedt, R.P. and Michels, H.J. 1989. Deflagration to detonation transitions and strong deflagrations in alkane and alkene air mixtures. *Combust. Flame,* 76,169.

Lindstedt, R.P. and Sakhitharan, V. 1998. Time resolved velocity and turbulence measurements in turbulent gaseous explosions. *Combust. Flame,* 114,469.

Lowesmith, B.J., Hankinson, G. and Johnson, D.M. 2011. Vapour cloud explosions in a long congested region involving methane/hydrogen mixtures. *Process Saf. Environ. Prot.,* 89, 234.

Ma, G., Li, J. and Abdel-Jawad, M. 2014. Accuracy improvement in evaluation of gas explosion overpressures in congestions with safety gaps. *J. Loss Prevent. Process Ind.,* 32, 358.

Mackay, D.J., Murray, S.B., Moen, I.O. and Thibault, P.A. 1989. Flame-jet ignition of large fuel-air clouds. *Proc. Combust. Inst.*, 22, 1339.

Mercx, W. P. M. 1992. Large-scale experimental investigation into vapour cloud explosions: comparison with the small-scale discoe trials. *Inst. Chem. Eng.,* 70 Part B, 197.

Moen, I.O., Donato, M., Knystautas, R. and Lee, J.H. 1980. Flame acceleration due to turbulence produced by obstacles. *Combust. Flame,* 39, 21.

Moen, I.O., Lee, J.H.S., Hjertager B.H., Fuhre, K. and Eckhoff, R.K. 1982. Pressure development due to turbulent flame propagation in large-scale methane-air explosions. *Combust. Flame,* 47,31.

Moen, I.O., Sulmistras, A., Hjertager, B.H. and Bakke, J.R. 1988. Turbulent flame propagation and transition to detonation in large fuel-air clouds. *Proc. Combust. Inst.* 21, 1617.

Mol'kov, V.V., Agafonov, V.V. and Aleksandrov, S.V. 1997. Deflagration in a vented vessel with internal obstacles. *Combust. Explosion and Shock Waves,* 33, 418.
Na'inna, A.M. 2013. *Effects of obstacle separation distance on gas explosions*. PhD thesis, University of Leeds, UK.

Na'inna, A.M., Phylaktou H.N., and Andrews, G.E. 2016. Turbulent combustion parameters in gas explosions with two obstacles with variable separatin distance. In: *Proc. of the Eight International Seminar on Fire and Explosion Hazards (ISFEH8)*, USTC Press, Heifei.

Obara, T., Yajima, S.T. Yoshihashi And S. Ohyagi. 1996. A high-speed photographic study of the transition from deflagration to detonation wave. *Shock Waves,* 6, 205.

Pang, L., Zhang, Q., Wang, T., Lin, D.C. and Cheng, L. 2012. Influence of laneway support spacing on methane/air explosion shock wave. *Saf. Sci.,* 50, 83.

Peraldi, O., Knystautas, R. and Lee, J. H. 1988. Criteria for transition to detonation in tubes. *Proc. Combust. Inst.,* 21, 1629.

Phylaktou, H. and Andrews, G.E. 1991. The acceleration of flame propagation in a tube by an obstacle. *Combust. Flame,* 85, 363.

Phylaktou, H. and Andrews, G.E. 1995. Application of turbulent combustion models to explosion scaling. *Process Saf. Environ. Prot.,* 73, 3.

Phylaktou, H. N. 1993. *Gas explosions in long closed vessels with obstacles : a turbulent combustion study applicable to industrial explosions*. PhD thesis, University of Leeds.

Phylaktou, H.N. and Andrews, G.E. 1994. Prediction of the maximum turbulence intensities generated by grid-plate obstacles in explosion-induced flows. *Proc. Combust. Inst.,* 25, 103.

Porowski, R. and Teodorczyk, A. 2013. Experimental study on DDT for hydrogen–methane–air mixtures in tube with obstacles. *J. Loss Prevent. Process Ind.,* 26, 374.

Robinson, G.F. and Kovitz, A.A. 1975. Efects of turbulence on pollutants formation in a tubular burner, *AAIA J.* 13,1488.

Robinson, H. and Wheeler, R.V. 1933. Explosions of methane and air: propagation through a restricted tube. *J. Chem. Soc.*, 758.

Rudy, W., Porowski, R. and Teodorczyk, A. 2011. Propagation of hydrogen-air detonation in tube with obstacles. *J. Power Technol.,* 91,122.

Sakthitharan, V. 1995. *Time-Resolved Measurements of Flame Propagation over Baffle-type Obstacles*. PhD thesis, University of London.

Sun, J., Liu, Y., Wang, Q. and Chen, P. 2005. Experimental study on interference effect of rarefaction wave on laminar propagating flame. *Chinese Sci. Bulletin*. 50, 919.

Tan-Atichat, J., Nagib, H. M. and Loehrke, R. I. 1982. Interaction of free-stream turbulence with screens and grids: a balance between turbulence scales. *J. Fluid Mech.,* 114, 501.

Taylor, G. I. 1946. The Air Wave Surrounding an Expanding Sphere. *Proc. R. Soc. London, Ser. A.* 186, 273.

Taylor, P.H. and Hirst, W.J.S. 1989. The scaling of vapour cloud explosions: a fractal model for size and fuel type, In: *22nd Proc. Combust. Inst. (Poster Presentation).*

Teodorczyk, A., Drobniak, P. and Dabkowski, A. 2009. Fast turbulent deflagration and DDT of hydrogen–air mixtures in small obstructed channel. *Int. J. Hydrogen Energy,* 34, 5887.

Teodorczyk, A., Lee J.H.S. and Knystautas, R. 1989. Propagation mechanism of quasi-detonations. *Proc. Combust. Inst.,* 22, 1723.

Ugarte O.J., Bychkov, V., Jad, S., Valiev, D. and Akkerman, V. 2016. Critical role of blockage ratio for flame acceleration in channels with tightly spaced obstacle. *Phys. Fluids* 28, 1.

Vollmer, K.G., Ettner, F. and Sattelmayer, T. 2011. Deflagration-to-detonation transition in hydrogen-air mixtures with concentration gradients. *In: 23rd International Colloquium on Dynamics of Explosions and Reactive Systems*, Irvine.

Wang, C., Huang, F., Kwasi Addai, E. and Dong, X. 2016. Effect of concentration and obstacles on flame velocity and overpressure of methane-air mixture. *J. Loss Prevent. Process Ind.,* 43, 302.

Ward Smith, A. J. 1971. *Pressure losses in ducted flows* (Ed). Butterworths,London.

Ward Smith, A. J. 1980. *Internal fluid flow (*Ed.*).* Clarendon press, Oxford.

Yang, X., Yu, M., Zheng, K., Luan, P. and Han S. 2020. An experimental study on premixed syngas/air flame propagating across an obstacle duct. *Fuel*, 267.

Yu, L.X., Sun, W.C. and Wu, C.K. 2002. Flame acceleration and overpressure development in a semiopen tube with repeated obstacles. *Proc. Combust. Inst.,* 29, 321.

Zhou, D.W. and Lee, S.J. 2004. Heat transfer enhancement of impinging jets using mesh screens. *Int. J. Heat Mass Transfer,* 47, 2097.

Zipf Jr, R., Gamezo, V.N., Mohamed, K.M., Oran, E.S. and Kessler, D.A. 2014. Deflagration-to-detonation transition in natural gas-air mixtures. *Combust. Flame*, 161, 2165.